

Stress-strain relationships of concrete damaged by freezing and thawing cycles

T. Ueda, M. Hasan, K. Nagai & Y. Sato
Hokkaido University, Sapporo, Japan

ABSTRACT: This study attempted to develop models for stress-strain relationships in tension and compression of concrete damaged by freezing and thawing cycles (FTC). Concrete specimens in shapes of cylinders and prisms were tested with the ASTM FTC test and in an environmental chamber where temperature and moisture conditions can be controlled as desired. After a certain number of FTC, the specimens were mechanically loaded and concrete strains were carefully measured. The test results indicate a rather linear relationship between the reduced dynamic elastic modulus and the reduced tensile strength and stiffness. The reduction in compression is different from that in tension. There is no longer linear relationship between the dynamic elastic modulus and the reduction of compressive strength. Instead the reduction in both strength and elastic modulus shows a rather linear dependency with the plastic tensile strain caused by FTC. Therefore, the stress-strain relationship under compression of FTC-damaged concrete is formulated as a function of remaining tensile strain caused by FTC. The stress-strain relationship under tension is formulated as a function of relative dynamic elastic modulus. In addition, numerical simulation with meso-scale material models was conducted and the results show good prediction of the reduction on strength and stiffness of FTC-damaged concrete.

Keywords: stress-strain relationship, freezing and thawing cycles, relative dynamic elastic modulus, FTC equivalent plastic strain, zero strength elements

1 INTRODUCTION

Frost damage in concrete is a typical environmental action that directly causes deterioration in the mechanical properties of concrete. Standardized measures, namely freezing and thawing tests, can quantify the deterioration. However method to quantify deterioration of concrete mechanical properties such as strength and stiffness due to freezing and thawing cycles (FTC) has not been developed yet.

Hasan et al. (1992) investigated the degradation of concrete strength and stiffness after being exposed to FTC in water (based on ASTM C666-92) and reported that for concrete without air-entraining (AE) agent, the strength and stiffness both in tension and compression reduces as increasing the number of FTC. For concrete with AE agent, no reduction on tensile strength and stiffness was found after being exposed to 305 cycles, but compressive strength and stiffness

reduces as increasing the number of FTC. The same phenomenon in compression for concrete with and without AE agent exposed to FTC in air was also reported (Hasan 2003, Hasan et al. in print). The remaining plastic tensile strain induced by FTC (or FTC equivalent plastic strain) can be a good parameter to predict the degradation of compressive strength and stiffness of FTC-damaged concrete (Hasan et al. 2003, Hasan et al. in print).

Based on the experimental results, stress-strain models both in tension and compression including the tension softening stage for concrete that has been affected by FTC are proposed. The models proposed in this study are based on the elasto-plastic and fracture model for concrete under mechanical plane stress states proposed by Maekawa & Okamura (1983). The model can be applied for concrete with and without AE agent. The proposed models are meant for application to a non-linear two-dimensional finite element program.

Analyses of notched plain concrete beams are conducted to verify the reliability of the models. The computed results are compared with those of the experimental results.

Numerical simulation with meso-scale material models is also conducted to predict the reduction on strength and stiffness of FTC-damaged concrete.

2 EXPERIMENTAL PROGRAM

2.1 Outline of specimens

Several concrete specimens with and without AE agent were prepared. High-early-strength Portland cement was used. The outline of specimens is shown in Table 1.

Table 1. Outline of specimens

Series	w/c	AE agent ^{*)}	Type	Size cm	TP	AT days
BN	0.5	0.00	Prism	10 × 10 × 40	A	30
BA	0.5	0.05	Prism	10 × 10 × 40	A	30
CN	0.5	0.00	Cylinder	φ10 × 20	B	50
CA	0.6	0.25	Cylinder	φ10 × 20	B	300
BEN	0.5	0.00	Prism	10 × 10 × 40	B	50

^{*)} Portion of AE agent by Portland cement weight (in %); TP = test procedure; AT = age of specimen when the FTC test started.

Mix proportions of the specimens are shown in Table 2. The specimens were demolded after 24 hours, and then cured in the water with the temperature around 20 °C. After the age of 28 days for series BN and BA; 25 days for series CN; 287 days for series CA; and 22 days for series BEN; the specimens were taken out from the water curing.

Table 2. Mix proportion of concrete specimens

Series	Cement kg	Water kg	Gravel kg	Sand kg	AW cc	AE cc	AC %
BN	320	160	1165	777	0	0	2.25
BA	320	160	1165	777	0	160	5.00
CN	320	160	1165	777	0	0	1.50
CA	267	160	1116	869	668	4	4.50
BEN	320	160	1165	777	0	0	1.50

AW=air entraining water reducer agent, AE=air entraining agent, AC=air content

2.2 Freezing and thawing test procedures

As shown in Table 1, specimens of series BN and BA were exposed to FTC test procedure A. The procedure A in this study was according to ASTM C666-92, which is FTC test in water. Freezing and thawing tests were started when the age of the specimens was 30 days as shown in Table 1. After the expected number of FTC the specimens were

taken out from the freezing and thawing chamber and then the dynamic elastic modulus tests were performed.

Specimens of series CN, CA and BEN were exposed to FTC test procedure B. This test procedure was freezing and thawing test in air introduced in a climate chamber at Hokkaido University where temperature and moisture conditions can be controlled as desired. On the surface of specimens of series CN, CA, and BEN, four strain gages were mounted to obtain the strain in axial and lateral directions.

Freezing and thawing test began in the climate chamber when the age of the specimens was 50 days except of series CA for which it was 300 days as shown in Table 1. The chamber temperature was controlled by 2 temperature sensors located in the chamber and connected to a computer. Before the test the chamber temperature was kept at 20 °C. And to keep the moisture content in the specimens, water was sprayed on the specimens for 15 minutes when the input temperature reached 19 °C during thawing of each FTC.

2.3 Mechanical loading test procedures

Three point bending tests were performed for series BN, BA and BEN with a notch on the center of the beam after exposed to certain number of FTC to evaluate tension softening curve as proposed by Niwa et al. (2000). The notch with the width of 4 mm and length of 50 mm was made by using a sawing machine. Two displacement transducers were placed at the plates that were attached at both ends of loading bar located at the center of the specimen and two others on the top of the specimen at the supporting points. Four π -gages were mounted along the ligament portion at each side of specimen to obtain the longitudinal strain distribution. These π -gages were placed at distances of 12.5 mm, 25 mm, 37.5 mm, and 50 mm from the top of the specimen respectively. The specimens were loaded with displacement control to obtain the complete load-deflection curve until the specimens separated into two halves. The splitting tests on cylinder specimens were also performed to find out the tensile strength.

Compression monotonic and unloading-reloading tests were performed on cube specimens (size of 100 mm) that were cored out from the notched beam specimens of series BN and BA. Six strain gages were placed on the cube specimens to obtain the axial and lateral strains.

Compression tests on specimens of series CA and CN were conducted in the climate chamber after being exposed to certain number of FTC.

Compression load was applied on the specimens with displacement control through an actuator. To measure the plastic strain and unloading stiffness, unloading-reloading test was performed. During the compression test, the chamber and specimen's temperatures were set at 20 °C.

3 TEST RESULTS

3.1 Plastic tensile strain under FTC

Under the effect of FTC, plastic tensile strain was observed at the end of cycles. The test results show that plastic tensile strains in axial and lateral directions are almost the same.

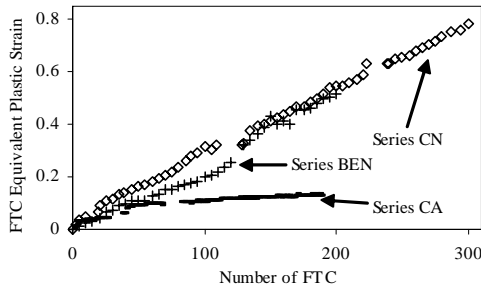


Figure 1. FTC equivalent plastic strain.

Here the term “FTC equivalent plastic strain” is used instead plastic tensile strain in axial and lateral direction. The equivalent strain (E) is a non-dimensional strain invariant, which is the function of two-dimensional mean and deviatoric strains (ε_m and γ_d) as follows (Maekawa & Okamura 1983, Hasan 2003, Hasan et al. in print):

$$E = \sqrt{\left(\frac{0.62}{\varepsilon'_{co}} \varepsilon_m\right)^2 + \left(\frac{0.98}{\varepsilon'_{co}} \gamma_d\right)^2} \quad (1)$$

where ε'_{co} is compressive strain at the uni-axial compressive strength. The FTC equivalent plastic strain increases as the number of FTC increases, as shown in Figure 1. The FTC equivalent plastic strain for air-entrained concrete (series CA) is observed to be much lower than that for the non air-entrained concrete (series CN and BEN).

3.2 Mechanical properties of FTC-damage concrete

As a result of damage of concrete during FTC, the mechanical properties such as strength and stiffness decay. Figures 2 and 3 show the degradation of compressive strength (f'_c), static elastic modulus in

compression (E_c), relative dynamic elastic modulus (d), tensile strength (f_t) and static elastic modulus in tension (E_t) as a function of FTC equivalent plastic strain (E_{pf}).

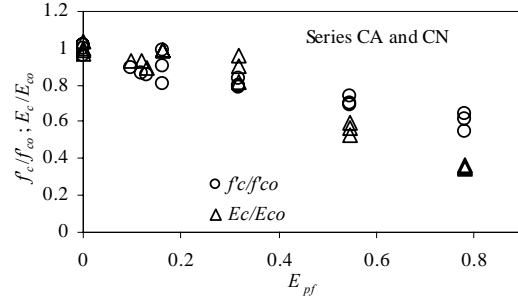


Figure 2. Reduction of compressive strength and stiffness as a function of FTC equivalent plastic strain.

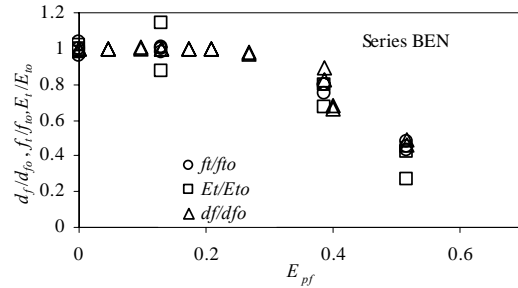


Figure 3. Reduction of relative dynamic elastic modulus, tensile strength and stiffness as a function of FTC equivalent plastic strain.

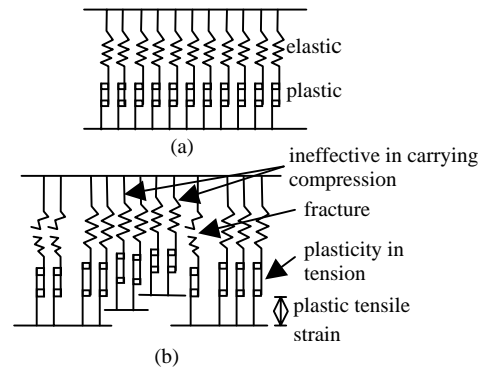


Figure 4. Concrete is assumed to be constructed by some of constituent elements; (a) Group of constituent elements; (b) Fracture and plasticity of some constituent elements during FTC.

The tensile strength and dynamic elastic modulus was still same as original concrete up to the FTC equivalent plastic strain of around 0.24 and reduced for the following increasing of FTC equivalent plastic strain. In the case of compression, it is

considered that the plasticity in tension during FTC causes non-plastic part of concrete ineffective to carry compression and results in the reduction of compressive strength and static elastic modulus as seen in Figure 4 (as also reported by Hasan et al. 2002, Hasan 2003, Hasan et al. 2003, Hasan et al. in print). The reason why the reduction in strength and stiffness was observed only in compression when FTC equivalent plastic strain is small may be found by conducting numerical analysis with consideration of the change in micro-structure in concrete due to FTC. Some attempt was made in Chapter 6.

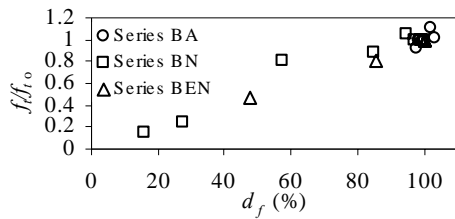


Figure 5. Reduction of tensile strength as a function relative dynamic elastic modulus.

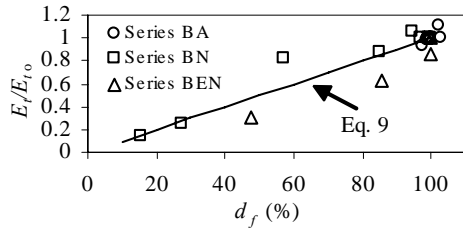


Figure 6. Reduction of tensile stiffness as a function relative dynamic elastic modulus.

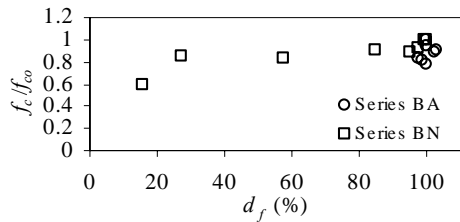


Figure 7. Reduction of compressive strength as a function relative dynamic elastic modulus.

From the experimental results, it can be concluded that the behavior of FTC-damaged concrete in tension and compression is different. The reduction of compressive strength and stiffness can be associated with the increment of FTC equivalent plastic strain. However, the reduction of tensile strength and stiffness should be associated

with the crack occurring during FTC indicated by reduction of relative dynamic elastic modulus. The relationships between degradation of tensile strength and stiffness and relative dynamic elastic modulus are shown in Figures 5 and 6. These figures show that reduction of tensile strength and stiffness is proportional. Figure 7 shows that there is no good relationship between reduction of compressive strength and relative dynamic elastic modulus.

4 STRESS-STRAIN MODEL FOR FTC-DAMAGED CONCRETE

4.1 Model for FTC-damaged concrete subjected to compression

In this model, concrete is assumed to be constructed by a group of constituent elements which are arranged in parallel as shown in Figure 4a.

Under the effect of FTC, it is assumed that some of the elements fracture and lose their ability to carry compression load due to microcracking (Fig. 4b). The fracture parameter to consider the damage caused by FTC is introduced besides the fracture parameter for mechanical loading proposed by Maekawa and Okamura (1983). From here the fracture parameter under the effect of FTC is referred to as “FTC fracture parameter” while the fracture parameter under the effect of mechanical loading as “mechanical fracture parameter”. The FTC fracture parameter represents the reduction of initial stiffness resulting from fracture of some elements as a concrete is damaged during FTC (see Fig. 4b). The FTC fracture parameter (β) is considered to be a function of FTC equivalent plastic strain. By fitting the experimental data shown in Figure 8, the relationship between FTC fracture parameter and FTC equivalent plastic strain can be given as follows;

$$\beta = e^{-0.45 E_{pf} (1 - e^{-30 E_{pf}})} \quad (2)$$

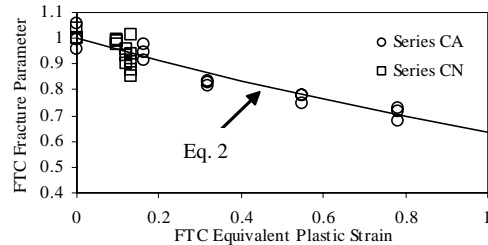


Figure 8. Formulation of FTC fracture parameter.

The microcracking also causes plastic tensile strain in the constituent elements as shown in Figure 4b. Because of the plastic tensile strain occurring in some elements, the non-fracturing elements whose plastic tensile strains are less cannot effectively carry the compression load. Those ineffective elements, however, can resume its load carrying ability once compressive strain cancels the plastic tensile strain. Accordingly, it is necessary to take an effective factor, α besides the fracture parameter to represent these phenomena. The effective factor is considered to be a function of FTC equivalent plastic strain (E_{pf}) and maximum mechanical equivalent strain (E_{max}) as follows;

$$\alpha = e^{-1.70E_{pf}} e^{1.70E_{pf}^{0.15} E_{max}^{0.85}} \text{ for } E_{max} < E_{pf} \quad (3)$$

$$\alpha = 1.0 \text{ for } E_{max} \geq E_{pf}$$

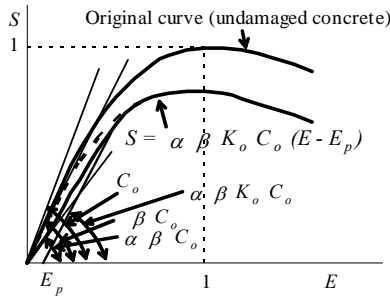


Figure 9. Equivalent stress-equivalent strain relationship for FTC-damaged concrete.

As a result, the mechanical equivalent stress-mechanical equivalent strain relationship for FTC damaged concrete can be written as follows (Fig. 9);

$$S = \alpha \beta K_o C_o (E - E_p) \quad (4)$$

where S is mechanical equivalent stress, E is mechanical equivalent strain, C_o is initial stiffness for S - E relationship, which is equal to 2.0, E_p is mechanical equivalent plastic strain and K_o is mechanical fracture parameter as follows;

$$K_o = e^{-0.73E_{max}} (1 - e^{-1.25E_{max}}) \quad (5)$$

As the damage in concrete by FTC increases, the mechanical equivalent plastic strain also increases. This phenomenon happens because the higher the damage is, the lesser compression the elements carry. These elements reach their plastic point more quickly resulting in a higher mechanical plastic

strain at the same maximum equivalent strain level. In this model, therefore, the mechanical equivalent plastic strain is also considered to be a function of not only the maximum mechanical equivalent strain but also the FTC equivalent plastic strain as follows;

$$E_p = E_{max} - a(1 - e^{-bE_{max}}) \quad (6)$$

where

$$a = \frac{20}{7} - 2.10E_{pf} + 0.34E_{pf}^2 \quad (7)$$

$$b = 0.35 + 0.25E_{pf} + 0.18E_{pf}^2$$

Using the presented model, the stress-strain curves for all specimens tested in this study were calculated. A good correlation between the calculated and experimental results was obtained. The comparison of maximum compressive stresses is shown in Figure 10. Figure 11 shows the comparison of stress-strain relationships for 2 groups of series CN.

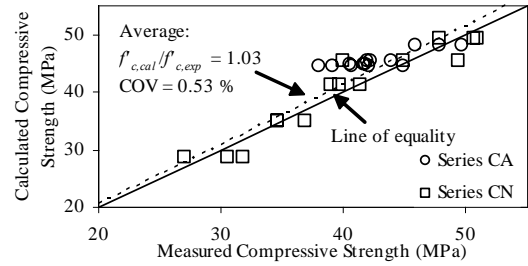


Figure 10. Comparison between calculated and measured compressive strength.

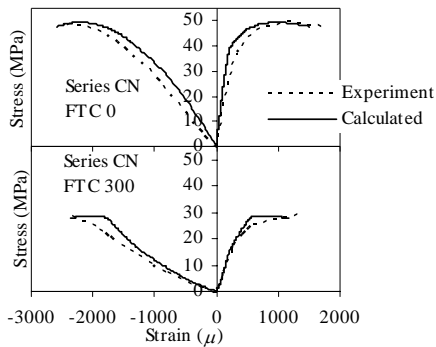


Figure 11. Comparison between calculated and experimental stress-strain curves.

4.2 Model for FTC-damaged concrete subjected to tension

Under tension, formation of crack in concrete is started if the fracture strength is exceeded. This

crack will propagate by continuing the applied tensile stress (Hillerborg et al. 1976). In this model, the crack is assumed to propagate when the stress in the crack tip reaches the tensile strength f_t . When the crack opens the stress is not assumed to fall to zero at once, but to decrease by increasing crack width w . Before the tensile strength is reached, the stress-strain relationship is assumed linear. The relationship between tensile stress-strain before crack propagation is given in the following equation;

$$\sigma_t = E_t \varepsilon_t \quad (8)$$

where E_t is tensile secant stiffness of concrete.

It is also assumed that the concrete constituent element has a strength distribution. Under the effect of FTC, some of the elements reach their fracture strength and then the internal crack starts to open. This results in the strength and stiffness degradation on the whole concrete. The stiffness for FTC damaged concrete (E_t) is considered to be a function of relative dynamic elastic modulus (d_f) as follows (see Fig. 6);

$$E_t = E_{t0} (d_f)^{1.012} \quad (9)$$

where E_{t0} is stiffness for undamaged concrete.

The tensile stress-crack width relationship after crack formation is formulated based on the experimental results as follows;

$$\sigma_t = E_t \varepsilon_{t0} \left\{ \left[1 + \left(7 \frac{w}{w_{max}} \right)^3 \right] e^{-19 \left(\frac{w}{w_{max}} \right)^3} - 0.2 \left[\left(\frac{w}{w_{max}} \right)^2 - \left(\frac{w}{w_{max}} \right) \right] \right\} \quad (10)$$

where ε_{t0} is tensile strain related to maximum tensile stress and w_{max} is maximum crack width (crack width at all tensile strain has been released).

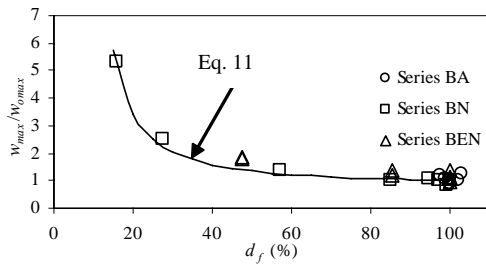


Figure 12. Maximum crack width.

Similar to the stiffness, the maximum crack width for damaged concrete is considered as a function of the relative dynamic elastic modulus and formulated as follows (Fig. 12);

$$w_{max} = w_{o,max} (0.73e^{0.31/d_f}) \quad (11)$$

where $w_{o,max}$ is the maximum crack width for the original concrete (non damaged concrete).

5 FINITE ELEMENT ANALYSIS

A non-linear finite element computer program (HUCOM) was used to analyze the notched concrete beams tested in this study. The program was developed based on the WCOMR (Okamura & Maekawa 1991). The eight-node quadratic elements were used. Each element contains 3x3 Gauss points. The model developed in this study was applied.

The comparison between the analytical and experimental maximum load for all groups of concrete specimens tested in this study is shown in Figure 13. The figure shows that the maximum load predicted by using the models developed in this study has a good agreement with the experimental data.

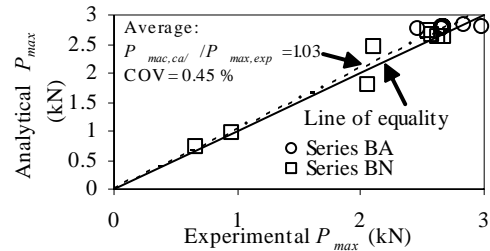


Figure 13. Comparison between analytical and experimental maximum load.

The load-deflection relationships for 7 specimens in series BA and 8 specimens in series BN were calculated. The results show a good relation between analytical and experimental load-deflection curves. Figure 14 plots the comparison between analytical and experimental load-deflection curves for 2 specimens in both BA and BN. The load-deflection curve for concrete with AE agent after being exposed to 305 cycles is almost similar with the original concrete, but for concrete without AE agent shows very high degradation on the capacity and stiffness. It means for concrete with AE agent that there is no internal cracking induced by FTC at all. Since the concrete

without AE agent has many internal cracking after being exposed to FTC, it can carry a very low load compared with the original concrete.

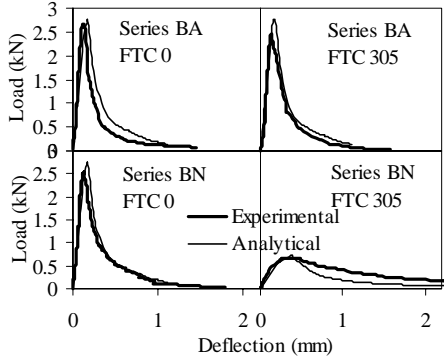


Figure 14. Comparison between analytical and experimental load-deflection curves.

6 SIMULATION WITH MESO-SCALE MODEL

Analysis with meso-scale material models was conducted to predict the degradation of concrete strength and stiffness both in tension and compression under the effect of FTC as well as the change in stress-strain curve. A two dimensional numerical simulation using Rigid Body Spring Method (RBSM) developed by Kawai and Takeuchi (1990) was used.

The meshing of analyzed model was realized by using a Voronoi diagram. The Voronoi diagram is the collection of Voronoi cells. Each Voronoi cell represents aggregate or mortar element in the analysis. For the Voronoi meshing, geometrical computation software developed by Sugihara (1998) was applied.

A strength distribution and meso-scale constitutive models proposed by Nagai et al. (2002) were applied. The tension softening model is linear with maximum crack width w_{max} . The program used for the analysis was developed by Nagai et al. (2002).

The analyzed model has dimension 100 mm \times 200 mm as shown in Figure 15. The number of meshing elements is 3046.

The fracture of element caused by FTC as described in Chapters 3 and 4 is considered by introducing zero strength elements since the fracturing elements have no ability to carry stress.

Figures 16 and 17 show the reduction on strength and stiffness in tension and compression as increasing the number of zero strength elements. The results indicated the proportional reduction of

tensile strength and its stiffness. It is very similar to the result of reduction of tensile strength and stiffness obtained by the experiment (Figs. 5 and 6).

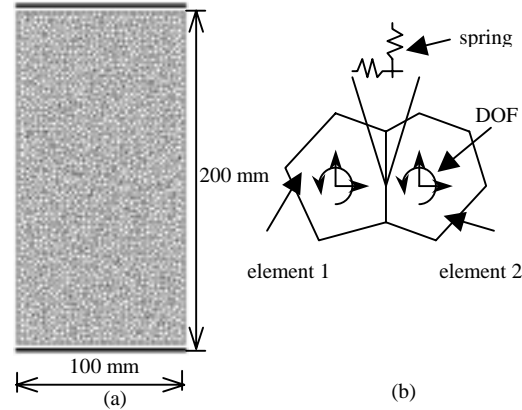


Figure 15. Analyzed model; (a) Meshing of analyzed model; (b) RBSM polygonal elements interconnected by springs and degrees of freedom (DOF).

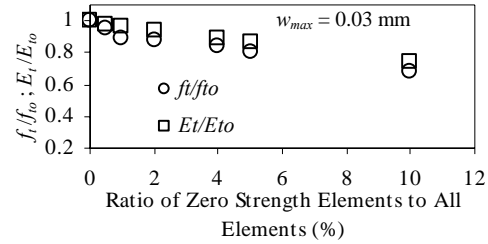


Figure 16. Reduction of tensile strength and stiffness as increasing the number of zero strength elements at $w_{max} = 0.003$.

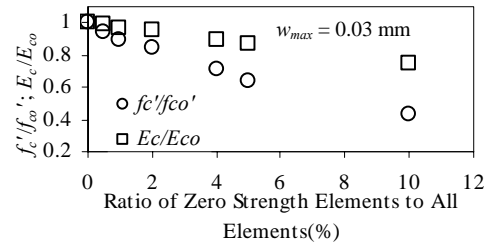


Figure 17. Reduction of compressive strength and stiffness as increasing the number of zero strength elements at $w_{max} = 0.003$.

Figure 17 shows that reduction of strength is higher than that of stiffness in compression. This stiffness degradation is only caused by fracture of element, which can be represented by β factor in the model presented in Chapter 4. However, further degradation of compressive initial stiffness was observed in the experiment, which is represented by a combination of two factors, α and β (see Fig.

9). To consider the reduction of initial stiffness caused by plasticity (α factor), the initial plastic tensile strain needs to be introduced in the meso-scale model in addition to the zero strength elements. The introduction of initial plastic strain in the meso-scale model is not discussed in this paper.

Another factor affecting the strength and stiffness reduction is the change in tension softening at a crack as shown in Sec. 4.2. The maximum crack width w_{max} , at which concrete tensile stress is totally released, was observed to increase with FTC (see Eq.(11) and Fig. 12). The increase in w_{max} increases in strength but stiffness (see Fig. 18). The authors believe that the combined effects of zero strength element, plastic tensile strain and increase in w_{max} could express the observed degradation in strength and stiffness in compression and tension. The results of further analysis will be presented in the near future.

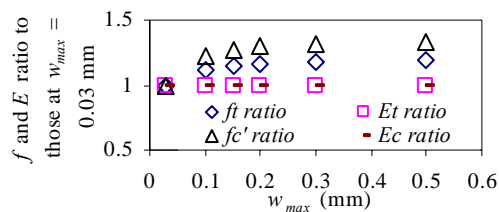


Figure 18. Effect of w_{max} on strength and stiffness (analytical results at ratio of zero strength elements to all elements = 5 %).

7 CONCLUSIONS

From this study, the following conclusions can be drawn;

1. The test results indicate that the tensile strength and elastic modulus in tension decrease linearly with the reduction of dynamic elastic modulus. The tension softening behavior of the concrete is also affected by freezing and thawing cycles (FTC). The crack width corresponding to the complete tensile stress release increases with the reduced dynamic elastic modulus.
2. The compression test shows the reduction in compressive strength and initial elastic modulus with increase in number of FTC. However, there is no longer linear relationship with the reduction in the dynamic elastic modulus. Instead the reduction in both strength and elastic modulus shows a rather linear dependency with the plastic tensile strain caused during FTC.
3. The stress-strain models in compression and tension of FTC-damaged concrete were developed. The stiffness degradation in tension was formulated as a function of relative dynamic

elastic modulus while in compression as a function of plastic tensile strain induced by FTC.

4. Using finite element method, some notch beam specimens damaged by FTC were analyzed to verify the reliability of the models. The calculated results show a good agreement with the experimental results.
5. Numerical simulation by rigid body spring method (RBSM) with meso-scale material models can express the strength and stiffness reduction in compression and tension, introducing elements with no strength, which represent the FTC damage. Other factors affecting the strength and stiffness are plastic tensile strain and change in tension softening model as observed in the experiment. The results of further study with RBSM will be presented.

8 REFERENCES

- Hasan, M., Nagai, K., Sato, Y. & Ueda, T. 2002. Stress-strain behavior in tension and compression of concrete damaged by freezing and thawing cycles. In: M.J. Setzer, R. Auberg & H.J. Keck (eds), *Frost Resistant of Concrete; Proc. intern. workshop, Essen 18-19 April 2002*: 197-204. Cachan Cedex: RILEM Publications S.A.R.L.
- Hasan, M. 2003. Modeling of stress-strain relationships for concrete damaged by freezing and thawing cycles. *PhD Dissertation*. Hokkaido University: Sapporo.
- Hasan, M., Okuyama, H. & Ueda, T. 2003. The damage mechanism and strain induced in frost cycles of concrete. *Japan Concrete Institute* 25 (1): 401-406.
- Hasan, M., Okuyama, H., Sato, Y. & Ueda, T. in print. Stress-strain model of concrete damaged by freezing and thawing cycles. *Advanced Concrete Technology*.
- Hillerborg, A., Modeer, M. & Petersson, P.E. 1976. Analysis of crack formation and crack growth in concrete by means of fracture mechanics and finite elements. *Cement and Concrete Research* 6 (6): 773-782.
- Kawai, T. & Takeuchi, N. 1990. *Discrete limit analysis program, series of limit analysis by computer 2 (in Japanese)*. Tokyo: Baihukan.
- Maekawa, K. & Okamura, H. 1983. The deformational behavior and constitutive equation of concrete using the elasto-plastic and fracture model. *J. of the Faculty of Engineering, the University of Tokyo (B)*, 37 (2): 253-328.
- Nagai, K., Sato, Y. & Ueda, T. 2002. Numerical simulation of fracture process of plain concrete by rigid body spring method. *Concrete Structure in 21st Century. Vol 8: Proc. of the first fib Congress*, Osaka: 99-106
- Nagai, K., Sato, Y., Ueda, T. & Kakuta, Y. 2002. Numerical simulation of fracture process of concrete model by rigid body spring method. *Japan Concrete Institute* 24 (2): 163-168.
- Niwa, J., Sumranwanich, T. & Matsuo, T. 2000. Experimental study to determine the tension softening curve of concrete. *Concrete Library International* 35: 1-18.
- Okamura, H. & Maekawa, K. 1991. *Nonlinear analysis and constitutive models of reinforced concrete*. Tokyo: Gihodo Shuppan.
- Sugihara, K. 1998. *Fortran computational geometry programming (in Japanese)*. Tokyo: Iwanami Shoten.